Stored Energy Based 3D Antenna Analysis and Design

Cismasu, Marius; Tayli, Doruk; Gustafsson, Mats

2014

CODEN:LUTEDX/(TEAT-7231)/1-18/(2014)

Stored Energy Based 3D Antenna Analysis and Design

Marius Cismasu, Doruk Tayli, and Mats Gustafsson

Electromagnetic Theory
Department of Electrical and Information Technology
Lund University
Sweden

Marius Cismasu
Marius.Cismasu@eit.lth.se

Department of Electrical and Information Technology
Electromagnetic Theory
Lund University
P.O. Box 118
SE-221 00 Lund
Sweden

Doruk Tayli
Doruk.Tayli@eit.lth.se

Department of Electrical and Information Technology
Electromagnetic Theory
Lund University
P.O. Box 118
SE-221 00 Lund
Sweden

Mats Gustafsson
Mats.Gustafsson@eit.lth.se

Department of Electrical and Information Technology
Electromagnetic Theory
Lund University
P.O. Box 118
SE-221 00 Lund
Sweden

Editor: Gerhard Kristensson

Abstract

A method to estimate $Q_{Z'}$ of antennas from a single frequency current distribution is introduced. Three-dimensional (3D) antennas are studied using this single-frequency method and previous results on single-frequency Q-factor estimation and current optimization. Physical bounds on the D/Q-ratio are derived using the concept of optimum antenna current distribution in the studied situations. These bounds are used for an antenna placement analysis applied to a wireless device model. Furthermore, the performance of antennas optimized using a genetic algorithm is compared with physical bounds customized for each analyzed situation. A combination of antenna Q and $Q_{Z'}$ is used as optimization objective for a 3D radiating structure.

1 Introduction

Antenna Q can be computed from a single frequency current distribution on a radiating structure using the method presented in [12] and [10]; see also [13]. This method is based on expressing the electric and magnetic energies stored in the fields created, and the power radiated by an antenna in terms of the current [25]. The Q-factor estimation method is applied in a genetic algorithm and method of moments (GA/MoM), [17, 23], optimization procedure in [5, 6]. The concept of optimum antenna current distribution, [10], is used to assess the performance of GA-optimized radiating structures in [5, 6]. An ant colony optimization method generates antennas whose performance is compared with physical bounds in [24]. "Corner connections," a typical characteristic of metallic-patch-based genetically optimized antennas, can be avoided using methods such as random geometry refinement, [20], patch overlapping, [16], faulty-gene purging, [6], *etc.*

Here we extend the single-frequency Q-factor estimation concept to $Q_{Z'}$, a parameter introduced in [28]. A 3D structure is used to show that this parameter can have small values, *e.g.*, $Q_{Z'} \ll 1$ although $Q > 1$. The energy-based single-frequency antenna Q estimation method is applied to the single-band Q-factor optimization of 3D radiating structures with rectangular ground planes. These structures represent simplified models of common wireless communication terminals, more realistic compared to the planar models analyzed in [5, 6]. A GA/MoM, [17, 23], procedure optimizes antennas of such 3D structures for minimum Q-factor. This procedure uses an in-house MoM solver with variable change for integrating $1/R$ singularities [18]. The commercial electromagnetic solver ESI-CEM [7] is used to compute the input impedance of the optimized structures. A single resonance, [9, 28], or multiple resonance Brune synthesis model, [27], is employed to evaluate the Q-factor of the structures from their input impedance. The Q-factors obtained using the in-house and commercial solver agree to a large extent.

Optimum current densities, [10], in the sense of their D/Q ratio, are derived for the 3D structures studied in this paper. The D/Q ratio of an optimum antenna current, realizable or not, gives the physical bound on D/Q for a real structure, *i.e.*, having a physical current density. The Q-factors of genetically optimized antennas

are compared with Q-factors of optimum currents. The same conditions, *e.g.*, geometry, optimization region, dimensions, *etc.*, are used both in genetic optimization and current optimization. In this way the bounds are customized for the analyzed situation. Customized bounds and optimum currents are used in an antenna placement in wireless device study. The objective of this study is to determine the antenna location that maximizes the performance of the device, measured as D/Q-ratio or Q-factor.

The paper is organized as follows. A summary of the theory presented in [5, 10, 12] on the use of stored energies for antenna analysis and design is included in Section 2.1. The single frequency $Q_{\mathrm{Z}'}$ estimation method is presented in Section 2.2. The convex optimization formulation used to derive physical bounds on D/Q and D/Q-optimum currents is described in Section 2.3. Section 3 presents the numerical simulations performed in this paper and their results. Section 3.1 describes the general simulation setup. The performance and examples of GA/MoM optimized 3D structures are presented and compared with optimum-current performance in Section 3.2. Section 3.3 illustrates the fact that some antennas can have $Q_{\mathrm{Z}'} \ll 1$ even though $Q > 1$. An antenna placement situation is investigated using optimum currents and physical limitations in Section 3.4. The paper ends with conclusions in Section 4.

2 Stored Energies and Physical Bounds for Antenna Analysis and Design

2.1 Stored Energies

Practical antenna analysis and design is usually performed using numerical techniques that solve differential and/or integral equations describing an electromagnetic problem. Examples and details of numerical techniques for electromagnetics can be found in text books such as [15, 21], *etc.*, and references therein. Such techniques are based, in general, on a discretized computation domain. The method of moments (MoM) is a numerical method particularly appropriate for antenna analysis due to the fact that the discretized domain is the surface of the spatially finite radiating structure, [15]. We consider a structure discretized for analysis using an electric field integral equation (EFIE)-based MoM solver. The current density $\boldsymbol{J}$ excited on the surface of the structure is approximated in terms of the local basis functions $\boldsymbol{\psi}_p$ as

$$\boldsymbol{J}(\boldsymbol{r}) \approx \sum_{n=1}^{N} J_n \boldsymbol{\psi}_n(\boldsymbol{r}), \tag{2.1}$$

where $\boldsymbol{r}$ is the position vector, $\mathbf{J} = (J_1, J_2, \ldots, J_N)^{\mathrm{T}}$ is a column vector of complex, surface-current, expansion coefficients, and N is the number of basis functions used to approximate the current. The expansion coefficients are usually determined from the system of equations

$$\mathbf{ZJ} = \mathbf{V}, \tag{2.2}$$

where $\mathbf{V}$ is a column vector describing the feeding of the structure, and $\mathbf{Z}$ is the impedance matrix describing the structure, [14, 15, 21].

The electric and magnetic energies stored in the fields created by a radiating structure, [25], are approximated in terms of the discrete current density $\mathbf{J}$ as the quadratic forms, [10],

$$W_{\mathrm{e}} \approx \frac{1}{4\omega}\mathbf{J}^{\mathrm{H}}\mathbf{X}_{\mathrm{e}}\mathbf{J} \tag{2.3}$$

and

$$W_{\mathrm{m}} \approx \frac{1}{4\omega}\mathbf{J}^{\mathrm{H}}\mathbf{X}_{\mathrm{m}}\mathbf{J}, \tag{2.4}$$

where ω is the angular frequency, and $\mathbf{X}_{\mathrm{e}}$ and $\mathbf{X}_{\mathrm{m}}$ are the electric and magnetic reactance matrices, respectively. The power radiated by an antenna is, [8, 13, 22, 25],

$$P_{\mathrm{r}} \approx \frac{1}{2}\mathbf{J}^{\mathrm{H}}\mathbf{R}_{\mathrm{r}}\mathbf{J}, \tag{2.5}$$

where $\mathbf{R}_{\mathrm{r}}$ is the radiation resistance matrix. Equations (2.3), (2.4) and (2.5) can be used to compute the Q-factor of a lossless resonant or non-resonant antenna as, [5, 28],

$$Q = \frac{2\omega \max\{W_{\mathrm{e}}, W_{\mathrm{m}}\}}{P_{\mathrm{r}}} \approx \frac{\max\{\mathbf{J}^{\mathrm{H}}\mathbf{X}_{\mathrm{e}}\mathbf{J}, \mathbf{J}^{\mathrm{H}}\mathbf{X}_{\mathrm{m}}\mathbf{J}\}}{\mathbf{J}^{\mathrm{H}}\mathbf{R}_{\mathrm{r}}\mathbf{J}}. \tag{2.6}$$

The definition in the first part of (2.6) is equivalent to that in [1] for resonant antennas. An overview of expressions for the Q-factor of antennas can be found in [26]. Equation (2.6) expresses the Q-factor of an antenna in terms of the current density computed for a single frequency. The bandwidth of an antenna can be estimated using a single frequency simulation, [5], based on the inverse proportionality between the bandwidth and Q in a single resonance model, [9, 28]. Quadratic forms similar to those in (2.5) have been employed for antenna array optimization in free space in [14].

The expressions for $\mathbf{X}_{\mathrm{e}}$, $\mathbf{X}_{\mathrm{m}}$ and $\mathbf{R}_{\mathrm{r}}$ resemble the expression for the EFIE-based impedance matrix, $\mathbf{Z}$, commonly computed by MoM solvers [5, 10, 12]. An MoM algorithm with Galerkin's method, [14, 21], applied to a mixed-potential EFIE formulation computes the impedance-matrix elements, [15, 21],

$$Z_{mn} = \mathrm{j}\eta_0 \int_{\partial V}\int_{\partial V} \left(k\boldsymbol{\psi}_{m1}\cdot\boldsymbol{\psi}_{n2} - \frac{1}{k}\nabla_1\cdot\boldsymbol{\psi}_{m1}\nabla_2\cdot\boldsymbol{\psi}_{n2} \right) \frac{\mathrm{e}^{-\mathrm{j}kR_{12}}}{4\pi R_{12}}\,\mathrm{dS}_1\,\mathrm{dS}_2, \tag{2.7}$$

where η_0 is the free space impedance, $k = \omega/\mathrm{c}_0$ is the wave number, c_0 is the speed of light in free space, R_{12} is the distance between the integration points in the two integration domains, and V is the the volume occupied by the antenna, bounded by the surface ∂V. Note that due to the inner product operation performed in the MoM, *i.e.*, one integration over the surface ∂V, the SI unit for Z_{mn} is $\Omega\mathrm{m}^2$ and for the right-hand-side $\mathbf{V}$—Vm. The resemblance of $\mathbf{X}_{\mathrm{e}}$ and $\mathbf{Z}$ is illustrated by

expressing the elements of the electric reactance matrix [10, 25]

$$X_{\mathrm{e},mn} = \eta_0 \int_{\partial V}\int_{\partial V} \nabla_1 \cdot \boldsymbol{\psi}_{m1} \nabla_2 \cdot \boldsymbol{\psi}_{n2} \frac{\cos(kR_{12})}{4\pi k R_{12}} - \left(k^2 \boldsymbol{\psi}_{m1} \cdot \boldsymbol{\psi}_{n2} - \nabla_1 \cdot \boldsymbol{\psi}_{m1} \nabla_2 \cdot \boldsymbol{\psi}_{n2}\right) \frac{\sin(kR_{12})}{8\pi} \,\mathrm{dS}_1 \,\mathrm{dS}_2. \quad (2.8)$$

Similarly, $\mathbf{X}_\mathrm{m}$ and $\mathbf{R}_\mathrm{r}$ resemble $\mathbf{Z}$ as (2.8) resembles (2.7) [5, 10]. These similarities allow integrating the computation of $\mathbf{X}_\mathrm{e}$, $\mathbf{X}_\mathrm{m}$ and $\mathbf{R}_\mathrm{r}$ in EFIE-based MoM solvers with little computational effort.

The MoM matrices, $\mathbf{Z}$, $\mathbf{X}_\mathrm{e}$, *etc.*, are intrinsically suitable for some global optimization algorithms such as GA/MoM optimization, [17, 23], current optimization, [10], *etc.* In such algorithms the optimization time of some antenna parameters, *e.g.*, the bandwidth, may be reduced using the single frequency expression (2.6) for Q. In addition these matrices are suitable for current optimization [10] used to derive physical limitations.

2.2 Single Frequency $Q_{\mathrm{Z}'}$ Computation

Consider an antenna having the input impedance

$$Z_\mathrm{in}(k) = R_\mathrm{in}(k) + \mathrm{j}X_\mathrm{in}(k). \quad (2.9)$$

This antenna is tuned to achieve resonance at the wave number k_0 using a series-connected, ideal, lumped inductor or capacitor, as in [28]. The input impedance of the tuned antenna becomes

$$Z_\mathrm{in,t}(k) = Z_\mathrm{in}(k) + \mathrm{j}X_\mathrm{t}(k), \quad (2.10)$$

where

$$X_\mathrm{t}(k) = \begin{cases} \dfrac{-kX_\mathrm{in}(k_0)}{k_0} & X_\mathrm{in}(k_0) < 0 \\ \dfrac{-k_0 X_\mathrm{in}(k_0)}{k} & X_\mathrm{in}(k_0) > 0 \end{cases}. \quad (2.11)$$

At the resonance frequency the input impedance has only the real part, *i.e.*,

$$Z_\mathrm{in,t}(k_0) = R_\mathrm{in}(k_0). \quad (2.12)$$

The Q-factor of the antenna tuned to resonance, in a single-resonance model, can be approximated as [28]

$$Q_{\mathrm{Z}'}(k_0) \approx \frac{k_0 \left|Z'_\mathrm{in,t}(k_0)\right|}{2R_\mathrm{in}(k_0)}, \quad (2.13)$$

where prime denotes first derivative with respect to wave number. Note the change of variables $k = \omega/\mathrm{c}_0$, performed in order for Z_in to be expressed in terms of the same frequency variable as $\mathbf{Z}$, whose elements are (2.7). If the single resonance assumption does not hold, the derivative of the input impedance may approach zero such that $Q_{\mathrm{Z}'} \approx 0$.

We express $Q_{\mathrm{Z}'}$ in terms of the frequency derivative of the impedance matrix, $\mathbf{Z}'$, whose elements are given by

$$\frac{k\partial Z_{mn}}{\eta_0 \partial k} = \int_V \int_V \mathrm{j}\left(k^2 \boldsymbol{\psi}_{m1}\cdot\boldsymbol{\psi}_{n2} + \nabla_1\cdot\boldsymbol{\psi}_{m1}\nabla_2\cdot\boldsymbol{\psi}_{n2}\right)\frac{\mathrm{e}^{-\mathrm{j}kR_{12}}}{4\pi k R_{12}} + \left(k^2\boldsymbol{\psi}_{m1}\cdot\boldsymbol{\psi}_{n2} - \nabla_1\cdot\boldsymbol{\psi}_{m1}\nabla_2\cdot\boldsymbol{\psi}_{n2}\right)\frac{\mathrm{e}^{-\mathrm{j}kR_{12}}}{4\pi}\,\mathrm{dV}_1\,\mathrm{dV}_2. \quad (2.14)$$

Replace (2.10) and (2.11) in (2.13) to obtain

$$Q_{\mathrm{Z}'}(k_0) \approx \left|\frac{k_0 Z'_{\mathrm{in}}(k_0)}{2R_{\mathrm{in}}(k_0)} + \mathrm{j}\frac{|X_{\mathrm{in}}(k_0)|}{2R_{\mathrm{in}}(k_0)}\right|. \quad (2.15)$$

An MoM solver gives all quantities needed to evaluate (2.15) except Z'_{in}. This quantity is traditionally computed using a numerical approximation based on evaluating Z_{in} for two closely spaced frequencies. An alternative to this approach is presented in the following.

The input impedance derivative is expressed in terms of the input admittance. The admittance matrix is given by:

$$\mathbf{J} = \mathbf{Y}\mathbf{V} = \mathbf{Z}^{-1}\mathbf{V}. \quad (2.16)$$

This matrix defines the input impedance of the antenna using a voltage gap model of feeding edge elements:

$$Y_{\mathrm{in}} = \frac{\mathbf{V}^{\mathrm{T}}\mathbf{Y}\mathbf{V}}{V_{\mathrm{in}}^2}, \quad (2.17)$$

where V_{in} is the voltage applied across the gap. Note that in an EFIE mixed-potential formulation with Galerkin testing and basis functions defined on pairs of adjacent rectangular mesh elements, [15, 19, 21], we have: $V_f = V_{\mathrm{in}}\ell_f$, where a voltage gap is applied along basis function f, and ℓ_f is the length of the edge common to the two rectangles where $\boldsymbol{\psi}_f \neq \mathbf{0}$. We consider that the source is real-valued and frequency independent, *i.e.*, $\mathbf{V}' = \mathbf{0}$. The input impedance derivative becomes

$$Z'_{\mathrm{in}} = \left(\frac{1}{Y_{\mathrm{in}}}\right)' = -\frac{Y'_{\mathrm{in}}}{Y_{\mathrm{in}}^2} = -\frac{\left(\mathbf{V}^{\mathrm{T}}\mathbf{Y}\mathbf{V}\right)'}{V_{\mathrm{in}}^2 Y_{\mathrm{in}}^2} = -\frac{\mathbf{V}^{\mathrm{T}}\mathbf{Y}'\mathbf{V}}{V_{\mathrm{in}}^2 Y_{\mathrm{in}}^2}. \quad (2.18)$$

Consider the following equation:

$$\mathbf{0} = \left(\mathbf{Z}^{-1}\mathbf{Z}\right)' = \left(\mathbf{Z}^{-1}\right)'\mathbf{Z} + \mathbf{Z}^{-1}\mathbf{Z}'. \quad (2.19)$$

Multiplication from the right by $\mathbf{Z}^{-1}$ gives

$$\mathbf{Y}' = -\mathbf{Z}^{-1}\mathbf{Z}'\mathbf{Z}^{-1} = -\mathbf{Y}\mathbf{Z}'\mathbf{Y}, \quad (2.20)$$

such that the input impedance derivative is

$$Z'_{\mathrm{in}} = \frac{\mathbf{J}^{\mathrm{T}}\mathbf{Z}'\mathbf{J}}{V_{\mathrm{in}}^2 Y_{\mathrm{in}}^2}, \quad (2.21)$$

where the fact that $\mathbf{Z}$ and $\mathbf{Y}$ are symmetric matrices has been used. Replace (2.21) in (2.15) to obtain

$$Q_{\mathrm{Z}'}(k_0) \approx \left| \frac{k_0 Z_{\mathrm{in}}^2(k_0) \mathbf{J}^{\mathrm{T}} \mathbf{Z}' \mathbf{J}}{2R_{\mathrm{in}}(k_0) V_{\mathrm{in}}^2} + \mathrm{j} \frac{|X_{\mathrm{in}}(k_0)|}{2R_{\mathrm{in}}(k_0)} \right|, \tag{2.22}$$

where the first derivative with respect to wave number of the impedance matrix, $\mathbf{Z}'$, is computed for the wave number k_0. The corresponding expression for $Q_{\mathrm{Z}'}$ in [4] differs from (2.22) as the former includes frequency derivatives of the current density and complex conjugates. An expression similar to (2.22) can be derived using a parallel tuning susceptance.

2.3 Physical Bounds

Physical bounds customized for the antennas analyzed can be derived by formulating appropriate optimization problems for antenna parameters [10]. These problems determine optimum antenna current densities in the sense of the parameter(s) of interest. Optimum antenna currents may or may not be physically realizable, *i.e.*, there may or may not exist a feeding scheme of the antenna that produces the optimum current. However, optimum currents give an upper bound on the performance a physical structure can achieve. One of the advantages of current optimization is the fact that customized bounds are derived without restrictive assumptions, *e.g.*, bounding geometry, electrical size, *etc.*

We use a convex optimization formulation for maximizing the partial directivity Q-factor ratio, D/Q, of radiating structures. This formulation is obtained by relaxation of, [10],

$$\begin{aligned} &\text{minimize}_{\mathbf{J}} \quad \max\{\mathbf{J}^{\mathrm{H}} \mathbf{X}_{\mathrm{e}} \mathbf{J}, \mathbf{J}^{\mathrm{H}} \mathbf{X}_{\mathrm{m}} \mathbf{J}\} \\ &\text{subject to} \quad \mathbf{F}^{\mathrm{H}} \mathbf{J} = -\mathrm{j}, \end{aligned} \tag{2.23}$$

to the dual problem, [3],

$$\begin{aligned} &\text{minimize}_{\mathbf{J}} \quad \mathbf{J}^{\mathrm{H}} \left(\alpha \mathbf{X}_{\mathrm{e}} + (1-\alpha) \mathbf{X}_{\mathrm{m}} \right) \mathbf{J} \\ &\text{subject to} \quad \mathbf{F}^{\mathrm{H}} \mathbf{J} = -\mathrm{j}, \end{aligned} \tag{2.24}$$

over $0 \leq \alpha \leq 1$. The solution of (2.24) for a fixed α is

$$\mathbf{J} = \frac{-\mathrm{j} \left(\alpha \mathbf{X}_{\mathrm{e}} + (1-\alpha) \mathbf{X}_{\mathrm{m}} \right)^{-1} \mathbf{F}}{\mathbf{F}^{\mathrm{H}} \left(\alpha \mathbf{X}_{\mathrm{e}} + (1-\alpha) \mathbf{X}_{\mathrm{m}} \right)^{-1} \mathbf{F}}, \tag{2.25}$$

with appropriate scaling of $\mathbf{J}$ such that $\mathbf{F}^{\mathrm{H}} \mathbf{J}$ is dimensionless. The $N \times 1$ matrix $\mathbf{F}$, with the elements

$$F_n^* = \frac{-\mathrm{j} k \eta_0}{4\pi} \int_V \hat{\boldsymbol{e}}^* \cdot \boldsymbol{\psi}_n(\boldsymbol{r}) \mathrm{e}^{\mathrm{j} k \hat{\boldsymbol{k}} \cdot \boldsymbol{r}} \, \mathrm{dV}, \tag{2.26}$$

is used to approximate the far field, $\boldsymbol{F}$, in the fixed direction $\hat{\boldsymbol{k}}$, projected on the polarization vector, $\hat{\boldsymbol{e}}$, as

$$\hat{\boldsymbol{e}}^* \cdot \boldsymbol{F}(\hat{\boldsymbol{k}}) \approx \mathbf{F}^{\mathrm{H}} \mathbf{J}. \tag{2.27}$$

Formulation (2.24) minimizes the energy stored in the fields created by a radiating structure for a fixed partial radiation intensity in a specific direction. Current densities optimum in the sense of (2.24) give the physical limitation on D/Q. The Q-factors of these currents, (2.6), may not be optimum in the sense of the Q-factor, *i.e.*, there may exist current densities producing smaller Q values. One advantage of formulation (2.24) and its solution (2.25) is the fact that there exist algorithms that solve (2.24) fast and efficiently even for large matrices and multiple directions and polarizations. For example the MATLAB function `fminbnd` can be used to solve (2.24).

3 Results

3.1 Simulation Setup

An in-house EFIE-based MoM solver computes the matrices $\mathbf{Z}$, $\mathbf{X}_\mathrm{e}$, $\mathbf{X}_\mathrm{m}$ and $\mathbf{R}_\mathrm{r}$ that describe the antennas studied. These matrices are used in GA/MoM as mother matrices [17], and for current optimization [10].

The in-house MoM-solver is based on Galerkin's method and a mixed-potential EFIE-formulation [14, 15, 21]. The basis and testing functions have a "rooftop" profile on pairs of adjacent rectangular mesh elements, *i.e.*, rectangles sharing a common edge [19], as illustrated in Fig. 1. Such a function has the amplitude linearly increasing toward the common edge and the direction from the first to the second rectangle (numbered according to a fixed mesh element numbering rule). The change of variable described in [18] is used to integrate the $1/R$ singularity for identical and closely spaced mesh elements.

An in-house genetic algorithm [5, 6] is employed for searching realistic structures with performance close to physical limitations. An initially-random, 200-individual, antenna population is improved according to evolutionary principles in steps. At each step 80 randomly chosen individuals compete to become one of two breeding parents. The resulting two offspring are affected by two-point cross-over (which happens 80 % of the time) and single-gene mutation (20 % probability). These offspring are placed in the population, which is enlarged by two. The antennas in this expanded population are ranked according to their fitness. The two least-fit antennas are removed from the population. Fitness is evaluated as an objective (cost) function that is minimized during optimization. This function is a combination of antenna parameters with different weights. After 300 consecutive steps without population improvement the algorithm enters a phase where the offspring produced always have up to 4 genes mutated. This phase is meant to reduce the solution time of the GA (however, this time improvement has not been studied). Once improvement is observed, the algorithm returns to "natural" conditions, single-gene mutation with 20 % probability. The optimization is stopped after $2\ 10^5$ steps or when genetic stability during $2\ 10^4$ steps is observed.

The commercial electromagnetic solver ESI-CEM [7] is used to verify the results obtained using the in-house solver through genetic optimization. This commercial

solver uses a triangular element mesh for discretizing the surfaces of analyzed structures. The results of a GA/MoM-optimized antenna ESI-CEM simulation are used to calculate the cost function for that antenna. In this way a comparison between the results obtained using the in-house solver and the commercial solver ESI-CEM is possible.

3.2 Bent-End Simple Phone Model

We consider infinitely-thin, lossless, perfect-electrical-conductor (PEC) structures in vacuum. The analyzed structures are spatially confined to three rectangular regions connected together as illustrated in Fig. 1. The first region has the length ℓ_1 and width $w = 7\,\text{cm}$. This region is the fixed ground plane, [5, 6]. The second and third rectangular regions, with the lengths ℓ_2 and $\ell_3 = 0.7\,\text{cm}$, respectively, and width w, represent the antenna region, [5, 6]. The lengths ℓ_1 and ℓ_2 are chosen such that $\ell_1 + \ell_2 = \ell = 14\,\text{cm}$. The region with the length ℓ_3 extends in a direction perpendicular to the common plane of the other two regions. This arrangement models, in a simplified manner, some common mobile terminals.

Three situations of the above arrangement are considered. The structures corresponding to these situations have $\ell_2 = 0.7\,\text{cm}$, $1.4\,\text{cm}$ and $2.8\,\text{cm}$, *i.e.*, 5 %, 10 % and 20 % of ℓ, respectively. The ground plane is fixed and metallic (PEC). The antenna region is used for current optimization—to derive physical limitations, and for genetic optimization—to find realistic structures approaching their physical limitations. Physical limitations are derived using convex optimization formulation (2.24) for the D/Q-ratio for each situation, [10]. Antennas are optimized for minimum Q through the GA/MoM optimization procedure, [17, 23].

The mother structure, [17, 23], corresponding to the arrangement described above consists of three infinitely thin PEC rectangular surfaces with the lengths ℓ_1, ℓ_2 and ℓ_3, and width w arranged as in Fig. 1. This structure is discretized with a non-uniform mesh, finer in the antenna region than in the ground plane for all situations considered. The first $11.2\,\text{cm}$ in the ℓ-direction from the left in Fig. 1 are divided in 40 mesh elements (and 25 in the w-direction). The remaining $2.8\,\text{cm}$ in the ℓ-direction are divided in 20 mesh elements (and 50 in the w-direction). The bent region is divided in 5 by 50 mesh elements in the ℓ_3 and w directions, respectively. This particular choice of discretization results in square mesh elements with the side $1.4\,\text{mm}$ in the antenna region and $2.8\,\text{mm}$ in the ground plane. A row of overlapping basis functions in the ℓ-direction at the place of the discontinuity in the mesh size couples electrically the regions with different discretizations.

The mother matrices, *i.e.*, the matrices $\mathbf{Z}$, $\mathbf{X}_\text{e}$, *etc.*, describing the mother structure, are square with 4435 rows. A block matrix decomposition is applied to these matrices, [17]. This decomposition reduces the sizes of the matrices manipulated repetitively during the GA/MoM optimization. These latter matrices are square with 990, 1485 and 2475 rows respectively for $\ell_2 = 0.7\,\text{cm}$, $1.4\,\text{cm}$ and $2.8\,\text{cm}$.

The genetic optimization of antenna Q has been run for five frequencies, given by $\ell/\lambda = 0.1,\ 0.2,\ 0.3,\ 0.4,$ and 0.5. Five optimized structures have been generated by the GA for each combination of ℓ_2 and frequency. The smallest optimized-structure

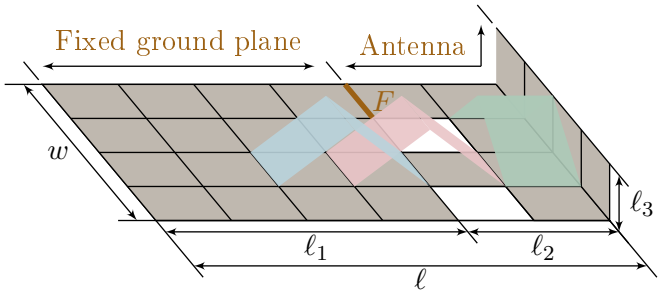

Figure 1: Illustration of rectangular mesh element discretization and "rooftop" basis function amplitude for a three-dimensional radiating structure. Metal areas are depicted in gray shading. The amplitudes of three of the total $7\times3+6\times4-4-3$ basis functions are depicted in blue, pink and green shading. The feeding edge is marked F.

Q-factor (2.6) of the five corresponding to each combination of ℓ_2 and frequency is labeled "Pred." in Fig. 2. The optimized structures with these smallest Q-factors (of which six are depicted in Fig. 3) have been simulated using the commercial solver ESI-CEM, [7]. The input impedance of these structures is used to obtain the Q-factors labeled "Sim." in Fig. 2. These Q-factors agree to a large extent with those obtained using the in-house MoM solver and the discrete expressions (2.3)–(2.6) (less than 6 % deviation relative to the former Q values). The single-resonance model described in [9, 28], (2.13), is employed to compute the Q-factor for $\ell/\lambda = 0.1$ and 0.2. The Q-factors for the other frequencies are computed using the multiple-resonance, Brune-synthesis model, [27]. The single-frequency $Q_{Z'}$ (2.22) has been applied to the structures having the smallest Q-factors mentioned above. The $Q_{Z'}$ values in these cases have less than 5 % difference relative to corresponding $Q_{Z'}$ values computed using (2.13).

The Q-factors obtained in optimization and simulation are compared to Q-factors given by optimum antenna current distributions, labeled "Opt." in Fig. 2. These distributions are obtained using the convex optimization formulation (2.24) for the D/Q-quotient, [10]. The matrices involved in these formulations are square with 990, 1485 and 2475 rows respectively for $\ell_2 = 0.7\,\text{cm}$, $1.4\,\text{cm}$ and $2.8\,\text{cm}$. These matrices are obtained using a uniform, 1.4 mm-side square mesh element discretization of the mother structure—same mother structure as that considered for GA optimization. The physical bound on the Q-factor of a rectangular PEC region with the dimensions $14 \times 7\,\text{cm}^2$ computed using the results in [11] is included for illustration. It is observed in Fig. 2 that the optimized-structure Q-factors are close to those achieved by optimum antenna currents (less than 13 % deviation relative to the optimum-current Q-factors). Note that the current distributions used to compute the curves labeled "Opt." in Fig. 2 are optimum in the sense of D/Q. However, the Q-factors computed from these distributions may not be optimum in the sense of the Q-factor. This may result in structures that are on the "wrong side" of the D/Q-optimum current Q-factor, *e.g.*, below the curves in Fig. 2. The D/Q-quotient of

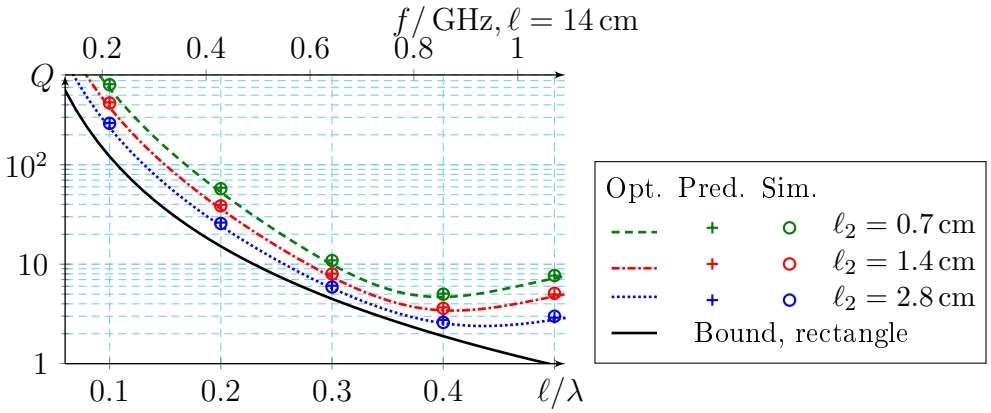

Figure 2: The Q-factors of antennas optimized using a genetic algorithm ("+") compared to corresponding Q-factors of D/Q-optimum current densities, [10], for the bent-end model illustrated in Fig. 1 with $\ell_2 = 0.7\,\mathrm{cm}$, $1.4\,\mathrm{cm}$ and $2.8\,\mathrm{cm}$ and $\ell = 14\,\mathrm{cm}$. The input impedance of the GA-optimized structures, computed by ESI-CEM, [7], has been used to calculate the Q-factors "$\circ$" using a resonance model [9, 27, 28]. The physical bound on Q for a rectangular PEC surface $14 \times 7\,\mathrm{cm}^2$, [11], is depicted in solid black line.

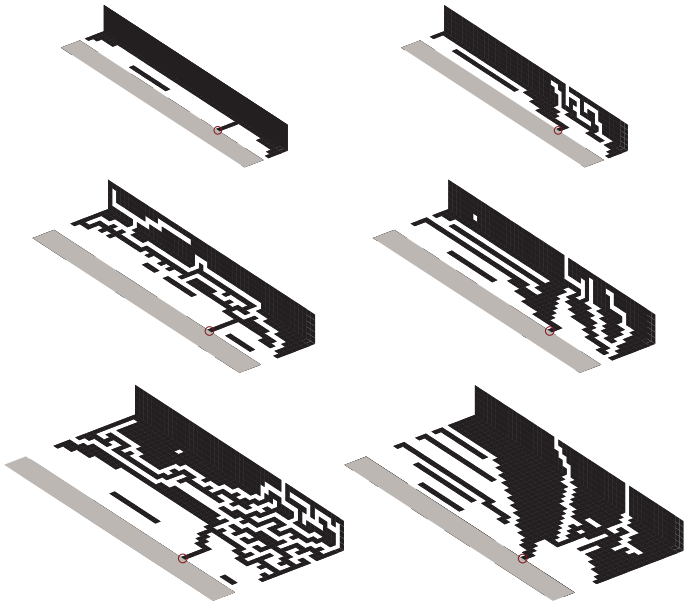

Figure 3: Example of genetic algorithm optimized structures (gray shading—part of the ground plane, black—antenna region part coplanar with the ground plane, bronze—antenna region part normal to the ground plane) with Q-factors depicted in Fig. 2 for $\ell/\lambda = 0.1$ (left column) and $\ell/\lambda = 0.5$ (right column), and $\ell_2 = 0.7\,\mathrm{cm}$ (top row), $1.4\,\mathrm{cm}$ (middle row), and $2.8\,\mathrm{cm}$ (bottom row). Feeding edges are circled.

such structures is on the "right side" of the physical bound.

3.3 Bent-End Simple Phone Model—Optimization for $Q_{Z'}$

The bent-end model with $\ell_1 = 12.6\,\text{cm}$ and $\ell_2 = 1.4\,\text{cm}$, described in Sec. 3.2, has been optimized using the GA for operation between 700 MHz and 960 MHz. This frequency band is divided in two sub-bands with the center frequencies $f_{c,1} = 759.5\,\text{MHz}$ and $f_{c,2} = 889.5\,\text{MHz}$, The fractional bandwidths of the two sub-bands are equal, $\text{FBW}_{1,2} \approx 15.8\,\%$. The matrices $\mathbf{Z}$, $\mathbf{X}_\text{e}$, $\mathbf{X}_\text{m}$ and $\mathbf{R}_\text{r}$ are computed for the center frequencies. Two extra impedance matrices are computed for the frequencies $1.001 f_{c,1,2}$ in order to evaluate $Q_{Z'}$ at $f_{c,1,2}$ using (2.13). The cost function minimized by the genetic algorithm is

$$F_\text{C} = \alpha_{\text{Q,M}} \max\left\{\frac{Q_1}{7} + \frac{Q_2}{7}\right\} + \alpha_{\text{Q,S}}\left(\frac{Q_1}{7} + \frac{Q_2}{7}\right) + \alpha_{\text{Q}_{Z'},\text{M}} \max\left\{Q_{Z',1} + Q_{Z',2}\right\} + \alpha_{\text{Q}_{Z'},\text{S}}\left(Q_{Z',1} + Q_{Z',2}\right), \quad (3.1)$$

where the indices 1 and 2 denote the sub-band, Q is the energy-based antenna-Q (2.6), $Q_{Z'}$ is the single-resonance input-impedance-derivative antenna-Q (2.13), and the weights α define the optimization target. The normalization values for Q, 7, ensure less than $-6\,\text{dB}$ reflection coefficient magnitude at the antenna input for the targeted FBW, under the assumption of single-resonance. The $Q_{Z'}$ values are not normalized because some applications target as low $Q_{Z'}$ as possible, *i.e.*, little variation of the input impedance in the operation band.

The GA has been run five times for each optimization target whose α-values are listed in Table 1. The Q-factors of the four GA-optimized structures depicted in Fig. 4 (of the total 15 structures) are presented in the same table. The structures corresponding to rows 1, 2 and 3 have the minimum cost function. The structure whose Q-factors are listed on row 4 has been optimized for simultaneous minimum Q and $Q_{Z'}$, does not have the minimum cost function, but has minimum Q on both sub-bands (out of the total 5 GA-optimized structures with this target). The values for $Q_{Z'}$ listed in Table 1 are evaluated with (2.13). These values agree to a large extent with the same values reevaluated at the center frequencies with (2.22). The four structures of Fig. 4 have been simulated in ESI-CEM [7]. The magnitudes of the reflection coefficients at the inputs of these structures are depicted in Fig. 5. Matching networks that yield less than $-6\,\text{dB}$ reflection coefficient in the entire band have been designed using BetaMatch [2]. These networks are depicted in Fig. 6 and the resulting S_{11} magnitudes in Fig. 5. Real component models of surface-mount device (SMD) lumped elements, including losses, have been used for matching.

3.4 Wireless Terminal Antenna Placement Analysis Using Optimum Currents

Optimum antenna currents can be employed for evaluation and comparison of the performance achievable by a device with antennas placed at different locations. For

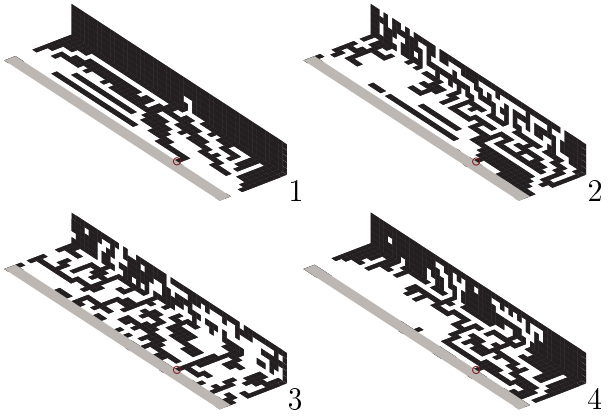

Figure 4: GA-optimized structures whose Q-factors are listed in Table 1. Gray shading—part of the ground plane, black—antenna region part coplanar with the ground plane, bronze—antenna region part normal to the ground plane. Feeding edges are circled.

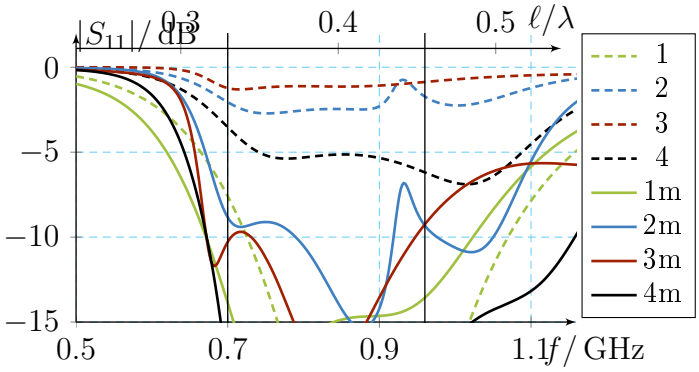

Figure 5: Magnitude of S_{11} at the input of the structures depicted in Fig. 4 without matching network, the curves labeled 1, 2, 3 and 4, and with the matching networks sketched in Fig. 6, the curves labeled 1m, 2m, 3m and 4m.

	Target	$\alpha_{Q,}$		$\alpha_{Q_{Z'},}$		Q_1	Q_2	$Q_{Z',1}$	$Q_{Z',2}$
		M	S	M	S				
1	min Q	1	0.1	0	0	4.6	3.7	2.9	0.3
2	min $Q_{Z'}$	0	0	1	0.1	8.2	8.9	0.01	0.01
3	min Q & $Q_{Z'}$	1	0.1	1	0.1	8.7	6.8	0.08	0.08
4						6.5	5.5	1.1	1.1

Table 1: GA cost function parameters and results for different optimization objectives

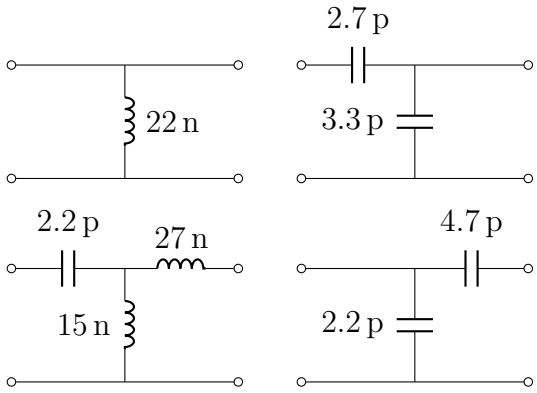

Figure 6: Matching networks designed for the structures depicted in Fig. 4 to yield less than −6 dB reflection coefficient magnitude between 700 . . . 960 MHz (solid curves in Fig. 5). Component values in SI units. Matching networks numbered as structures in Fig. 4—left to right and top to bottom.

illustration, we would like to determine the position and shape of the antenna region, [5, 6], that has the smallest Q-factor in the frequency range of Fig. 2. The nine 3D simplified models of common hand-held wireless terminals depicted in Fig. 7 are analyzed. These models are limited to a rectangular parallelepiped with the dimensions $\ell \times w \times h = 14 \times 7 \times 0.7\,\mathrm{cm}^3$ (*i.e.*, length × width × height). Note that limiting the structures to a parallelepiped is introduced for illustration purpose and does not restrict the applicability of the procedure exemplified here. Each model is drawn in Fig. 7 to scale in three side views from the ℓ, w and h-directions (except for Fig. 7h where an h-side view and two sections through the symmetry planes are depicted). Gray and black represent the ground plane and antenna region, respectively. The thickness of the infinitely thin PEC material is exaggerated.

The ground plane, [5, 6], consists of an infinitely thin planar PEC sheet that covers 90 % of the area of one $\ell \times w$ face of the parallelepiped bounding the antenna. The remaining 10 % of that face represents the support of the antenna region, which may be continuous or divided in more sub-regions. Here, a maximum of two sub-regions have been used. The structures in the antenna regions are limited to infinitely thin PEC sheets placed on faces of the 3D shape of the antenna region. This shape

Struct.	a	b	c	d	e, f	g	h	i
N	7584	8256	7568	7584	8256	8256	10830	7584
N_{AR}	1936	2608	1928	1944	2616	2612	5168	1992

Table 2: Dimensions of MoM matrices for the structures of Fig. 7

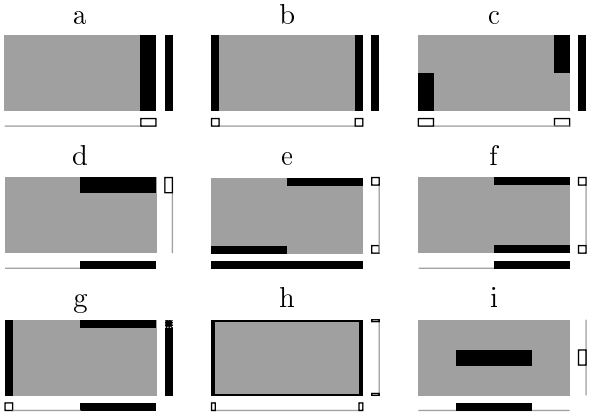

Figure 7: Nine simplified wireless-device models limited to a parallelepiped, consisting of a planar ground region extending 90 % of one length×width face, and an antenna region occupying 10 % of the parallelepiped volume. Three side views are depicted for a-g and i, *i.e.*, structures as seen along the length, width and height. A side view along the height and two sections at the symmetry planes are depicted for h. Gray shading—ground plane; black—antenna region, [5, 6].

is obtained by translating the 10 % of the $\ell \times w$-face area reserved for the antenna region a distance h perpendicularly to the ground plane (*i.e.*, by extruding the 10 % in the h-direction to the opposed face). The shapes resulting in the antenna region are made of rectangular parallelepipeds. These parallelepipeds are covered with PEC sheets on the four largest-area faces (in the case depicted in Fig. 7h there are four openings adjacent to the ground plane corners in the $w \times h$-plane; these are one mesh-element wide and extend the entire h-dimension).

The antenna region placement situations introduced above are discretized using a uniform mesh of $1.75 \times 1.75\,\mathrm{mm}^2$ rectangular elements. The total number of basis functions, N, resulting for the structures depicted in Fig. 7 are presented in Table 2 (*i.e.*, the number of rows and columns, where applicable, of $\mathbf{Z}$, $\mathbf{Z}'$, $\mathbf{X}_{\mathrm{e}}$, $\mathbf{X}_{\mathrm{m}}$, $\mathbf{R}_{\mathrm{r}}$, and $\mathbf{F}$). The same table presents the number of rows, and columns where applicable, N_{AR}, of the blocks, [17], corresponding to the 10 %-$\ell \times w$-area antenna region [5, 6]. These blocks are computed for the matrices involved in the convex optimization formulation (2.24).

The bounds on D/Q using formulation (2.24) for the simplified models of Fig. 7 are depicted in Fig. 8. Linear polarization along the length and directivity in the direction of the height of the parallelepiped bounding the models are considered. The

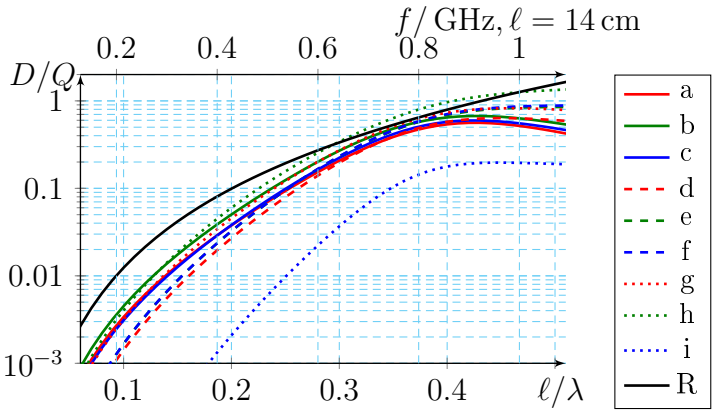

Figure 8: Physical bounds on D/Q for the structures depicted in Fig. 7 obtained using the convex optimization formulation (2.24), [10], when only the antenna region (black in Fig. 7) is optimized. The physical bound on D/Q for a rectangular PEC surface $14 \times 7\,\mathrm{cm}^2$, [11], is depicted in solid black line and labeled "R."

bound computed using the results in [11][1] for a rectangular, infinitely thin, $14\times7\,\mathrm{cm}^2$ PEC sheet is labeled "R" in Fig. 8. The D/Q-optimum current distributions giving the physical bounds in Fig. 8 are used to compute the Q-factors (2.6) depicted in Fig. 9. The physical bound on Q for a rectangular $14 \times 7\,\mathrm{cm}^2$ PEC sheet, [11], is labeled "R" in Fig. 9. The ring structure depicted in Fig. 7h outperforms all other structures in the figure in terms of D/Q and Q, except for a frequency region around $\ell/\lambda \approx 0.1$ where the structure in Fig. 7b has a greater D/Q. We also note that around $\ell/\lambda \approx 0.37$ a few of the structures in Fig. 7 reach close to the D/Q bound of a rectangular region and the structure in Fig. 7h has a D/Q value greater than that of a rectangular region. The optimum-current Q-factors do not reach as close to the physical bound on Q for a rectangular region as the D/Q-values.

4 Conclusions

A method to estimate $Q_{\mathrm{Z}'}$ of antennas from the current distribution computed for a single-frequency is introduced. This method and other previous results are applied to three analysis and design situations of three-dimensional radiating structures. These applications suggest that customized physical bounds, optimum currents, and single-frequency expressions such as (2.6), (2.22), are tools that may be useful for antenna design, *e.g.*, to stop an optimization process, assess realizability of specifications, assess performance of antenna locations, *etc.*

The first situation mentioned above is global optimization of 3D antennas with knowledge of physical bounds pertaining the radiating structure as it is, without assumptions such as electrical size, bounding geometry, *etc.* The results presented here suggest that single-frequency estimations such as (2.6) and (2.22) can reduce

[1] http://www.mathworks.se/matlabcentral/fileexchange/26806-antennaq

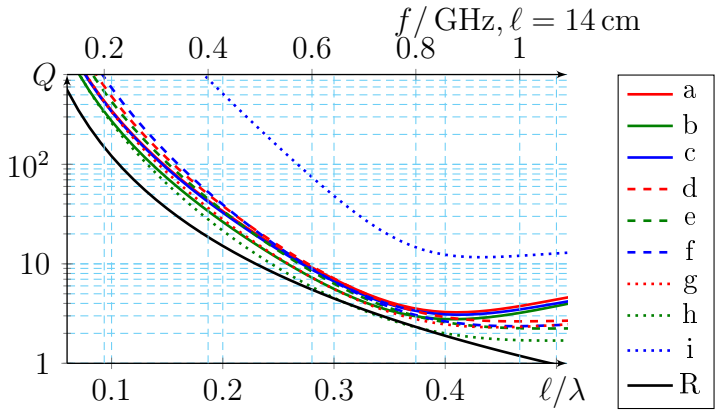

Figure 9: The Q-factors (2.6) achieved by the currents that give the optimum D/Q-values depicted in Fig. 8. The Q-factor of a $14 \times 7\,\mathrm{cm}^2$ PEC rectangle, [11], is labeled "R."

the optimization time of some antenna parameters, *e.g.*, antenna bandwidth, Q. Furthermore, carefully integrated physical bounds can be used for physical-limitation aware optimization, *i.e.*, to stop an optimization process when the target is achieved with a certain margin.

The second situation is a non-exhaustive study of optimizing antennas for Q versus $Q_{\mathrm{Z}'}$, or both. Four examples illustrate values for Q and $Q_{\mathrm{Z}'}$ obtained by antennas optimized genetically for Q, (2.6), $Q_{\mathrm{Z}'}$, (2.13), and both. The three targets include simultaneous operation on two different frequencies. The different frequencies can be centers of adjacent (as here) or separated frequency bands.

The third situation is the use of optimum antenna currents for determining the optimum position of an antenna in a wireless device. Nine simplified device models are analyzed, in which the antenna/antennas may occupy 10 % of the device volume. These models can be generated manually (as is the case here) or by an optimization process.

References

[1] Antenna Standards Committee of the IEEE Antennas and Propagation Society. IEEE Standard Definitions of Terms for Antennas, 1993. IEEE Std 145-1993.

[2] MNW Scan, Singapore—BetaMatch, Software for antenna component matching. http://www.mnw-scan.com/.

[3] S. P. Boyd and L. Vandenberghe. *Convex optimization*. Cambridge Univ Pr, 2004.

[4] M. Capek, L. Jelinek, P. Hazdra, and J. Eichler. The Measurable Q Factor and Observable Energies of Radiating Structures. *IEEE Trans. Antennas Propagat.*, **62**(1), 311–318, Jan 2014.

[5] M. Cismasu and M. Gustafsson. Antenna Bandwidth Optimization with Single Frequency Simulation. *IEEE Trans. Antennas Propagat.*, **62**(3), 1304–1311, 2014.

[6] M. Cismasu and M. Gustafsson. Multiband Antenna Q Optimization using Stored Energy Expressions. *IEEE Antennas and Wireless Propagation Letters*, **13**(2014), 646–649, 2014.

[7] ESI Group, Paris, France—ESI Group's computational electromagnetic (CEM) solution. http://www.esi-group.com.

[8] W. Geyi. *Foundations of Applied Electrodynamics*. John Wiley & Sons, 2011.

[9] M. Gustafsson and S. Nordebo. Bandwidth, Q-factor, and resonance models of antennas. *Progress in Electromagnetics Research*, **62**, 1–20, 2006.

[10] M. Gustafsson and S. Nordebo. Optimal antenna currents for Q, superdirectivity, and radiation patterns using convex optimization. *IEEE Trans. Antennas Propagat.*, **61**(3), 1109–1118, 2013.

[11] M. Gustafsson, C. Sohl, and G. Kristensson. Illustrations of new physical bounds on linearly polarized antennas. *IEEE Trans. Antennas Propagat.*, **57**(5), 1319–1327, May 2009.

[12] M. Gustafsson, M. Cismasu, and B. L. G. Jonsson. Physical bounds and optimal currents on antennas. *IEEE Trans. Antennas Propagat.*, **60**(6), 2672–2681, 2012.

[13] M. Gustafsson and B. L. G. Jonsson. Stored electromagnetic energy and antenna Q. Technical Report LUTEDX/(TEAT-7222)/1–25/(2012), Lund University, Department of Electrical and Information Technology, P.O. Box 118, S-221 00 Lund, Sweden, 2012. http://www.eit.lth.se.

[14] R. F. Harrington. *Field Computation by Moment Methods*. Macmillan, New York, 1968.

[15] J. M. Jin. *Theory and Computation of Electromagnetic Fields*. Wiley, 2011.

[16] M. John and M. Ammann. Wideband Printed Monopole Design Using a Genetic Algorithm. *Antennas and Wireless Propagation Letters, IEEE*, **6**, 447–449, 2007.

[17] J. M. Johnson and Y. Rahmat-Samii. Genetic algorithms and method of moments GA/MOM for the design of integrated antennas. *IEEE Trans. Antennas Propagat.*, **47**(10), 1606–1614, oct 1999.

[18] M. A. Khayat and D. R. Wilton. Numerical evaluation of singular and near-singular potential integrals. *IEEE Trans. Antennas Propagat.*, **53**(10), 3180–3190, October 2005.

[19] J. R. Mosig and F. E. Gardiol. A dynamical radiation model for microstrip structures. In P. W. Hawkes, editor, *Advances in Electronics and Electron Physics*, volume 59, pages 139 – 237. Academic Press, 1982.

[20] M. Ohira, H. Deguchi, M. Tsuji, and H. Shigesawa. Multiband single-layer frequency selective surface designed by combination of genetic algorithm and geometry-refinement technique. *IEEE Trans. Antennas Propagat.*, **52**(11), 2925–2931, Nov 2004.

[21] A. F. Peterson, S. L. Ray, and R. Mittra. *Computational Methods for Electromagnetics*. IEEE Press, New York, 1998.

[22] D. M. Pozar. Considerations for millimeter wave printed antennas. *IEEE Trans. Antennas Propagat.*, **31**(5), 740–747, September 1983.

[23] Y. Rahmat-Samii and E. Michielssen. *Electromagnetic Optimization by Genetic Algorithms*. Wiley Series in Microwave and Optical Engineering. John Wiley & Sons, 1999.

[24] M. Shahpari, D. Thiel, and A. Lewis. An Investigation Into the Gustafsson Limit for Small Planar Antennas Using Optimization. *IEEE Trans. Antennas Propagat.*, **62**(2), 950–955, Feb 2014.

[25] G. A. E. Vandenbosch. Reactive energies, impedance, and Q factor of radiating structures. *IEEE Trans. Antennas Propagat.*, **58**(4), 1112–1127, 2010.

[26] J. Volakis, C. C. Chen, and K. Fujimoto. *Small Antennas: Miniaturization Techniques & Applications*. McGraw-Hill, New York, 2010.

[27] O. Wing. *Classical Circuit Theory*. Springer, New York, 2008.

[28] A. D. Yaghjian and S. R. Best. Impedance, bandwidth, and Q of antennas. *IEEE Trans. Antennas Propagat.*, **53**(4), 1298–1324, 2005.